Tidal Destruction in a Low-mass Galaxy Environment: The Discovery of Tidal Tails around DDO 44*

Jeffrey L. Carlin , Christopher T. Garling , Annika H. G. Peter , Denija Crnojević , Duncan A. Forbes, Jonathan R. Hargis , Burçin Mutlu-Pakdil , Ragadeepika Pucha , Aaron J. Romanowsky , Duncan A. Forbes, Kristine Spekkens , Ragadeepika Pucha , Aaron J. Romanowsky , David J. Sand , Kristine Spekkens , July Strader , and Beth Willman , and Beth Willman , Kristine Spekkens , July Strader , and Beth Willman , and Beth Willman , and Beth Willman , LSST, 950 North Cherry Avenue, Tucson, AZ 85719, USA; jearlin@lsst.org, jeffreylearlin@gmail.com , 2 CCAPP and Department of Astronomy, The Ohio State University, Columbus, OH 43210, USA , and CCAPP, Department of Physics, and Department of Astronomy, The Ohio State University, Columbus, OH 43210, USA , and Lord , Usa , and Spec Telescope Science Institute, Symburne University, Hawthorn VIC 3122, Australia , Space Telescope Science Institute, 3700 San Martin Drive, Baltimore, MD 21218, USA , and Lord , Space Telescope Science Institute, 3700 San Martin Drive, Baltimore, MD 21218, USA , University of California Observatory, 933 North Cherry Avenue, Rm. N204, Tucson, AZ 85721-0065, USA , University of California Observatories, 1156 High Street, Santa Cruz, CA 95064, USA , Department of Physics & Astronomy, San José State University, One Washington Square, San Jose, CA 95192, USA , Department of Physics, Royal Military College of Canada, P.O. Box 17000, Station Forces, Kingston, On K7L 7B4, Canada , Department of Physics and Astronomy, Michigan State University, East Lansing, MI 48824, USA , Association of Universities for Research in Astronomy, 950 North Cherry Avenue, Tucson, AZ 85719, USA , Received 2019 June 19; revised 2019 October 3; accepted 2019 October 7; published 2019 November 26

Abstract

We report the discovery of a \gtrsim 1° (\sim 50 kpc) long stellar tidal stream emanating from the dwarf galaxy DDO 44, a likely satellite of Local Volume galaxy NGC 2403 located \sim 70 kpc in projection from its companion. NGC 2403 is a roughly Large Magellanic Cloud (LMC) stellar-mass galaxy 3 Mpc away, residing at the outer limits of the M81 group. We are mapping a large region around NGC 2403 as part of our Magellanic Analogs' Dwarf Companions and Stellar Halos survey, reaching point-source depths (90% completeness) of (g, i) = (26.5, 26.2). Density maps of old, metal-poor RGB stars reveal tidal streams extending on two sides of DDO 44, with the streams directed toward NGC 2403. We estimate total luminosities of the original DDO 44 system (dwarf and streams combined) to be $M_{i,\text{tot}} = -13.4$ and $M_{g,\text{tot}} = -12.6$, with \sim 25%–30% of the luminosity in the streams. Analogs of \sim LMC-mass hosts with massive tidally disrupting satellites are rare in the Illustris simulations, especially at large separations such as that of DDO 44. The few analogs that are present in the models suggest that even low-mass hosts can efficiently quench their massive satellites.

Unified Astronomy Thesaurus concepts: Dwarf spheroidal galaxies (420); Galaxy photometry (611); Galaxy interactions (600); Dwarf galaxies (416); Galaxy stellar halos (598); Tidal tails (1701)

1. Introduction

Deep surveys covering large sky areas have in recent years greatly expanded the number of dwarf galaxy satellites known around the Milky Way (MW; e.g., Drlica-Wagner et al. 2015, 2016; Kim & Jerjen 2015; Laevens et al. 2015; Torrealba et al. 2016, 2018; Homma et al. 2018) and M31 (e.g., Martin et al. 2016; McConnachie et al. 2018). The newly discovered diminutive galaxies include extremely low-luminosity "ultrafaint dwarfs" (UFDs; e.g., Willman et al. 2005; Belokurov et al. 2007—see the recent review by Simon 2019), as well as many relic streams from tidally disrupted satellites criss-crossing the Galactic halo (e.g., Belokurov et al. 2006; Grillmair & Carlin 2016; Shipp et al. 2018). In parallel to these discoveries, models of structure formation and evolution within the Λ -Cold Dark Matter (Λ CDM) framework have generated predictions of the number of satellites expected, as well as properties such as their luminosity functions and metallicities (Benson et al. 2002; Zolotov et al. 2012; Wetzel et al. 2016; Bose et al. 2018; Jethwa et al. 2018; Kim et al. 2018; Nadler et al. 2019). Although the match with the MW and M31—the only systems with robust samples of satellites—is remarkably good, it is

unclear whether our Galaxy and its nearest massive neighbor are representative of massive galaxies more generally, or if theoretical models are over-tuned to the Local Group. Resolved stellar maps of nearby massive galaxies are now being painstakingly assembled, revealing the satellite systems (down to the scale of UFD galaxies) of Cen A (Crnojević et al. 2019), NGC 253 (Sand et al. 2014; Romanowsky et al. 2016; Toloba et al. 2016), M81 (Chiboucas et al. 2013), M101 (Merritt et al. 2014; Bennet et al. 2017, 2019; Danieli et al. 2017; Müller et al. 2017), and M94 (Smercina et al. 2018), among others. We are thus entering an era in which we may explore the stochasticity of satellite populations around a variety of hosts, as well as their dependence on environment and host properties (e.g., Bennet et al. 2019). These can be used to make more precise tests of galaxy formation and the ΛCDM cosmological model

Of particular interest are satellites in less dense environments than the ones highlighted above. Satellites of the MW in particular show signs of experiencing many types of environmental quenching and disruption simultaneously (Barkana & Loeb 1999; Mayer et al. 2006; Greevich & Putman 2009; Nichols & Bland-Hawthorn 2011; Brown et al. 2014; Slater & Bell 2014; Fillingham et al. 2015; Wetzel et al. 2015). Because so many processes are likely to affect the satellites, it is often

^{*} Based on data collected at Subaru Telescope, which is operated by the National Astronomical Observatory of Japan.

difficult to assess their relative importance, and how that importance scales with properties of the host (not necessarily limited to halo mass). One way to disentangle these processes, and to highlight the scales at which each mechanism kicks in, is to consider low-mass hosts. Hosts inhabiting halos smaller than the MW's ought not to have hot-gas halos (Birnboim & Dekel 2003), so ram pressure stripping and possibly starvation may be significantly reduced compared to the MW (although they are likely to have cool circumgalactic media; Bordoloi et al. 2014). Moreover, they should have gentler tidal fields, reducing the effects of tidal heating and stripping. Thus, we expect satellite galaxies of low-mass hosts to be more like field galaxies, and less influenced by their environment. The environmental processes that are important for less massive hosts are likely to be different from those most relevant to MWsized galaxies. These hypotheses remain to be tested.

We have an additional motivation to study satellites of lowmass galaxies, in that many of the recently discovered dwarf galaxies within the MW halo are thought to have originated as satellites of the Large and Small Magellanic Clouds (LMC, SMC), and only recently fell into the MW (e.g., Jethwa et al. 2016; Dooley et al. 2017; Sales et al. 2017; Kallivayalil et al. 2018). The luminosity function of the new discoveries is unexpected, though—there are no massive $(M_* > 10^4 M_{\odot})$ MC satellite candidates (though Pardy et al. 2019 suggest that the Carina and Fornax dSphs may be associated with the MCs), but many that are much smaller, at odds with typical stellarmass-halo-mass relations (Dooley et al. 2017). 14 It is unknown whether the LMC and SMC had a more typical luminosity function at infall and many satellites have been stripped from them by the MW, or if this luminosity function is typical and is telling us something new about galaxy formation in small halos.

To extend the mass range of hosts for which satellite searches have been carried out to lower mass (Magellanic Cloud-mass) systems, without the difficulty of interpreting the interplay of the LMC and its satellites with the Galactic halo, we are conducting a census of nearby LMC stellar-mass analogs. With this survey-Magellanic Analogs' Dwarf Companions and Stellar Halos (MADCASH)—we are searching for the satellite populations of MC-mass galaxies within ~4 Mpc of the MW. Some early results from this ongoing survey include the discovery of the $M_V \sim -9.7$ dwarf galaxy Antlia B near NGC 3109 (Sand et al. 2015; Hargis et al. 2019), the detection of extended stellar populations around nearby galaxy IC 1613 (Pucha et al. 2019), and our discovery of a faint $(M_V \sim -7.7)$ satellite of NGC 2403 (Carlin et al. 2016). In this work, we highlight the discovery of a dwarf satellite being tidally disrupted around nearby ($D \sim 3.2 \,\mathrm{Mpc}$; Karachentsev et al. 2013) low-mass (stellar mass $M_* \sim 7 \times 10^9 M_{\odot}$; roughly 2 × LMC stellar mass) spiral galaxy NGC 2403, a relatively isolated system at the outskirts of the M81 group.

The dwarf spheroidal DDO 44 is a relatively massive dwarf ($M_R \sim -13.1$, similar to the Fornax satellite of the MW; Karachentsev et al. 1999) that is at a distance and velocity consistent with orbiting as a satellite of NGC 2403. Here we report evidence that the dwarf spheroidal DDO 44 has stellar tidal tails extending at least $\sim 0^{\circ}.5$ (~ 25 kpc) from its center. This discovery is based on data from our deep, wide-area

imaging survey to a projected radius of \sim 100 kpc around NGC 2403.

In Section 2, we introduce our discovery data set and analysis procedure. We show the key characteristics of the stream in Section 3. In Section 4, we discuss what the stream implies for the relationship between the orbital and star formation histories of DDO 44, and the frequency of small galaxy disruption by low-mass hosts. We highlight our key results in Section 5.

2. Data and Analysis

Deep imaging data were obtained with Hyper Suprime-Cam (HSC; Furusawa et al. 2018; Kawanomoto et al. 2018; Komiyama et al. 2018; Miyazaki et al. 2018) on the Subaru 8.2 m telescope. The 1°.5 diameter field of view of HSC corresponds to $\sim 80 \text{ kpc}$ at the $D \sim 3.0 \text{ Mpc}$ distance of NGC 2403, enabling a relatively efficient survey to beyond a projected radius of $d > 100 \,\mathrm{kpc}$ around NGC 2403 (a large fraction of the ~120-180 kpc virial radius of an isolated LMCmass analog; see, e.g., estimates of R_{vir} in Dooley et al. 2017). Our data consist of seven HSC pointings (see map in Figure 3): the CENTER, EAST, and WEST fields were observed on 2016 February 9–10, while the four additional HSC fields (NW, NE, SW, and SE) were observed 2017 December 23-24. All observations consist of 10×300 s exposures in the g band (known as "HSC-G" at Subaru) and $10 \times 120 \,\mathrm{s}$ in i ("HSC-I2"). We also observed short, 5×30 s sequences of exposures to improve photometry at the bright end. All observations from both runs were obtained in seeing between ~ 0.15 and 0.19, under clear skies.

The data were processed with the LSST pipeline, a version of which was forked to create the reduction pipeline for the HSC-SSP survey (Aihara et al. 2018a, 2018b). Details of the reduction steps can be found in Bosch et al. (2018). In short, we performed forced point-spread function (PSF) photometry on coadded frames in each filter, and calibrated both astrometrically and photometrically to PanSTARRS-1 (PS1; Schlafly et al. 2012; Tonry et al. 2012; Magnier et al. 2013). We applied extinction corrections based on the Schlafly & Finkbeiner (2011) coefficients derived from the Schlegel et al. (1998) dust maps. All results presented in this work are based on extinction-corrected PSF magnitudes.

For separation of point sources from unresolved background galaxies, we compare the ratio of PSF to cmodel fluxes for all sources, where the *cmodel* is a composite bulge/exponential plus de Vaucouleurs profile fit to each source. Point sources should have flux ratios $f_{PSF}/f_{cmodel} \sim 1$, while extended sources will contain additional flux in the model measurement that is not captured by the PSF. Figure 1 shows the *i*-band flux ratio as a function of i-band PSF magnitude. A large number of sources (especially at the bright end) are concentrated around unity in this figure. We allow for an intrinsic width of ± 0.03 in the flux ratio, and select sources whose 1σ uncertainties in flux ratio place them within this ± 0.03 window. The point-source candidates selected in this way are shown as red points in Figure 1, with extended sources (i.e., "not point sources") as gray points. Note that some background galaxies will contaminate the point-source sample below $i \sim 23$, where background galaxies far outnumber stars. For the remainder of this work we will analyze only this point-source sample calibrated to the PS1 photometric system.

¹⁴ A similar result is found for the MW as a whole (Kim et al. 2018).

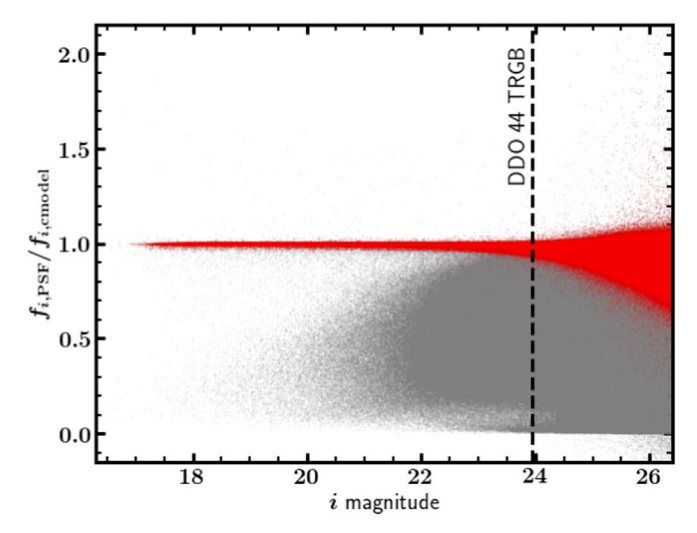


Figure 1. Star/galaxy separation based on the ratio of PSF to cmodel fluxes. The measured flux ratios of sources, $f_{i,PSF}/f_{i,cmodel}$, are shown as a function of i-band PSF magnitude; flux ratios of ~ 1 correspond to point-like sources. We classify all objects whose flux ratios are consistent (within their measured 1σ errors) with $f_{i,PSF}/f_{i,cmodel} \sim 1 \pm 0.03$ as point sources (i.e., "stars"). These are shown as red points above, with all other excluded sources shaded gray. For reference, our measured magnitude of the DDO 44 tip of the red giant branch (TRGB) is plotted as a dashed vertical line.

To characterize the completeness of our photometric catalog, we injected artificial stars into the images using Synpipe (Huang et al. 2018), which was written for HSC-SSP, and has been incorporated into the LSST pipeline. The resulting completeness (i.e., the fraction of artificial stars recovered by the photometric pipeline) in a 20' region centered on DDO 44 (excluding the central 2' where crowding is too extreme to resolve stars; a total of 18975 artificial stars were injected in this region, or $\sim 15 \, \mathrm{arcmin}^{-2}$) is given in Figure 2. We fit a function of the form given in Martin et al. (2016) to these curves, and estimate 50% (90%) completeness limits of i = 26.7 (26.2) and g = 27.5 (26.5). In the lower panels of the figure, we compare the input and recovered magnitudes for the artificial stars in both bands. These are centered on zero, so we are confident that no systematic offsets are present in our photometry.

3. A Stream Around DDO 44

One of the primary goals of our large-area imaging campaign around NGC 2403 is to search for its dwarf galaxy companions and/or the remnants of destroyed satellites. Thus one of the first things we did upon finishing the data reduction was to select stars with color-magnitude diagram (CMD) positions consistent with metal-poor RGB stars at the distance of NGC 2403, and plot their density on the sky. This RGB density map centered on NGC 2403 is shown in Figure 3. For the most part, the map shows a fairly uniform distribution over the entire region surveyed. This is most likely predominantly fore-/ background contamination, with little or no "halo" population in the outer regions around NGC 2403. We note that the 0.75 bins in this map are about the size of a typical faint dwarf galaxy at the distance of NGC 2403—1' ≈ 0.9 kpc at $D = 3.0 \,\mathrm{Mpc}$. Thus the faint dwarf galaxy MADCASH J074238+652501-dw found by Carlin et al. (2016) is almost completely contained in a single pixel of this map (approximately at $(\alpha - \alpha_0) \sim 0.5$ and $(\delta - \delta_0) \sim -0.2$), and thus not visible as an obvious overdensity. The most striking feature in

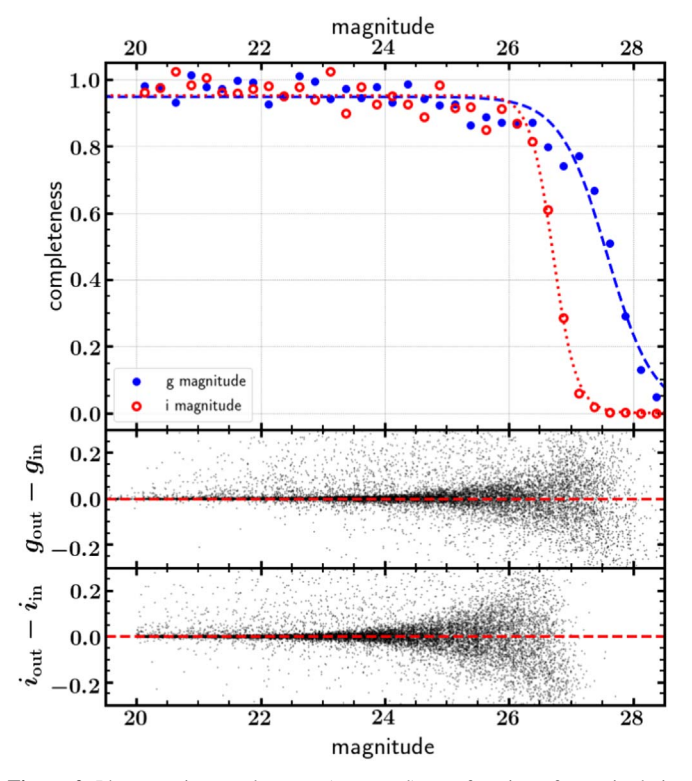


Figure 2. Photometric completeness (top panel) as a function of magnitude in the 20' region around DDO 44. The dashed and dotted lines show fits to the completeness curves of the form used in Martin et al. (2016); the data are 50% (90%) complete for point sources at i=26.7 (26.2) and g=27.5 (26.5). The lower panels compare recovered and input artificial star magnitudes, demonstrating that no systematic error is present in our photometric measurements.

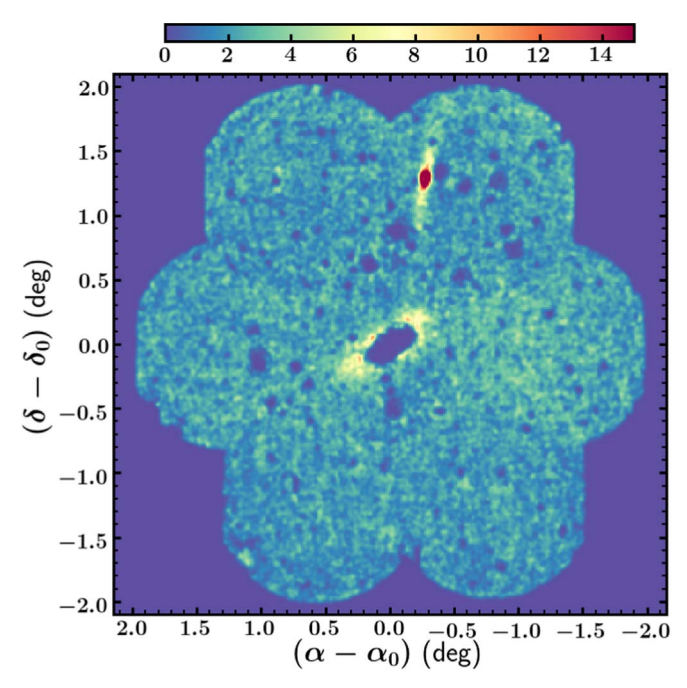


Figure 3. Density map of candidate RGB stars at the distance and metallicity of DDO 44/NGC 2403 (selected using the RGB box in Figure 4). Bins are 0.75, and the image has been smoothed with a Gaussian kernel of 0.75 FWHM. The field is centered on NGC 2403 (the hole in the center is due to extreme crowding), and DDO 44 is to the north (and slightly west). NGC 2366 is \sim 2.4 north of DDO 44. Stellar number densities have been corrected for completeness as a function of position; the color bar encodes the number of stars per 0.75 bin. North is up and east is to the left.

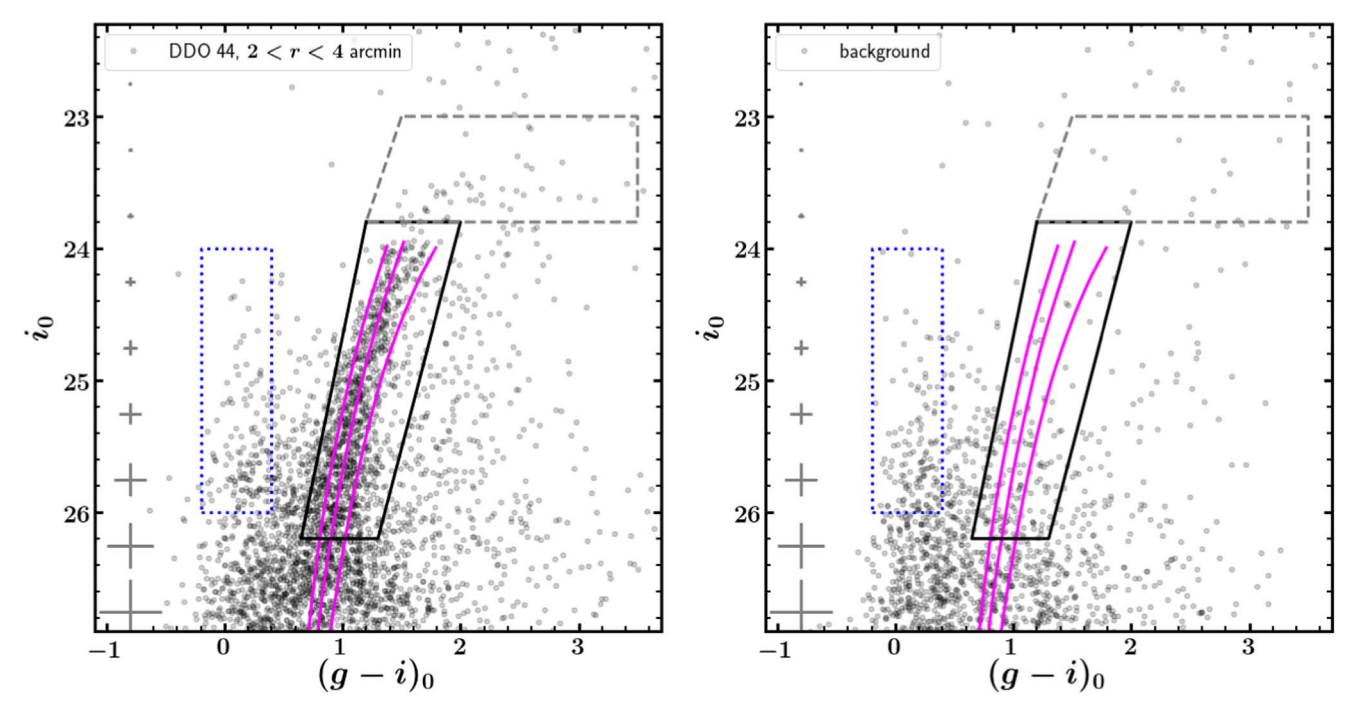


Figure 4. Left panel: color-magnitude diagram of stars between 2' and 4' of the center of DDO 44, showing a clearly defined old, metal-poor RGB of DDO 44, with few (if any) young stars. We exclude the region inside r < 2' because the photometry in this inner region is affected by crowding; blending and elevated background due to unresolved stars is also the source of the large scatter (especially redward of the RGB) in the DDO 44 CMD. We overlay MIST isochrones (Choi et al. 2016; Dotter 2016) for old (10 Gyr) populations with [Fe/H] = -1.6 (our estimate for the metallicity of DDO 44; see Section 3.1) flanked by isochrones with metallicities ± 0.5 dex, and shifted to our measured distance modulus of 27.36. The black box shows the selection used to isolate candidate RGB stars for all analysis in this paper. The other polygons outline regions used to select candidate AGB (dashed gray box) and blue sources (dotted blue outline) for Figure 5. Median photometric uncertainties as a function of magnitude are shown near the left edge of the plot. Right panel: CMD of sources in a region shifted southwest by 0.2 in both R.A. and decl., but of the same size as the DDO 44 field. This highlights (a) the lack of stars within the RGB box relative to the left panel, and (b) a similar population of sources within the blue box as seen in the DDO 44 CMD, suggesting that these are unresolved background galaxies rather than blue stars associated with DDO 44.

Figure 3 is the prominent blob corresponding to the known dwarf spheroidal galaxy DDO 44 to the north (and slightly west) of NGC 2403. Our deep Subaru+HSC data enable us to see for the first time that DDO 44 has streams of stars emanating from it, oriented along the direction toward (and away from) NGC 2403; i.e., DDO 44 is tidally disrupting beyond doubt.

3.1. TRGB Distance, Isochrone Fit

In Figure 4 (left panel) we show a CMD of all stars between 2' and 4' of the center of DDO 44. There is a prominent metalpoor RGB (highlighted by the solid black box) as well as a significant number of AGB stars (dashed gray box) signaling the presence of intermediate-age (\sim 2–8 Gyr old) stellar populations (as was found in Hubble Space Telescope (HST) imaging by Karachentsev et al. 1999 and Alonso-García et al. 2006). The dotted blue box in each panel denotes the location where young main-sequence stars would appear, if present. By comparing the DDO 44 field with an equal-area background region (right panel), the number of objects in this box is consistent with being background (likely unresolved galaxies/ QSOs, given their blue colors). In our later analysis, we show (e.g., the lower panel of Figure 5) that there is no concentration of blue sources at the position of DDO 44, confirming that these are background objects rather than young stars in DDO 44.

To refine the distance of DDO 44, we first selected stars with colors consistent with metal-poor RGB stars $(0.8 < (g - i)_0 < 2.1)$, and within 6' of the center of DDO 44. We binned these stars as a function of magnitude,

then convolved the luminosity function with a zero-sum Sobel edge-detection filter (in particular, one with values [-1.0, -2.0, -1.0, 0.0, 1.0, 2.0, 1.0], as in Jang & Lee 2017). We identify a narrow peak in the convolved luminosity function, corresponding to the tip of the RGB (TRGB), at $i_{\text{TRGB}} = 23.95 \pm 0.05$. From 10 Gyr Dartmouth isochrones (Dotter et al. 2008) at $[Fe/H] = -1.6 \pm 0.3$, we estimate an i-band TRGB absolute magnitude¹⁵ (in the PS1 system) of $-3.41^{+0.02}_{-0.01}$. We thus derive a distance to DDO 44 of $2.96 \pm 0.10 \, \mathrm{Mpc}$ (i.e., distance $(m - M)_0 = 27.36 \pm 0.07$). We note that the same TRGB code applied to the main body of NGC 2403 yields an identical distance modulus of $(m - M)_{N2403} = 27.36$. Our derived distance modulus is in agreement with other recent determinations for DDO 44 $((m - M)_0 = 27.39 \pm 0.13, 27.45,$ and 27.36 ± 0.09 ; Alonso-García et al. 2006; Dalcanton et al. 2009; Jacobs et al. 2009), though somewhat at odds with the value of $(m - M)_0 = 27.50$ given in the COSMICFLOWS-3 database (Tully et al. 2016).

At a distance of 2.96 Mpc, the on-sky separation between DDO 44 and NGC 2403 of 78.73 corresponds to a projected separation of \sim 67 kpc.

After determining the TRGB magnitude (and thus distance) of DDO 44, we wish to estimate the system's metallicity. To do so, we create a set of old (10 Gyr) Dartmouth isochrones in 0.1 dex metallicity intervals, and use a least-squares

 $[\]overline{^{15}}$ Note that the *i*-band TRGB magnitude is virtually independent of metallicity for metal-poor populations (as we confirmed with isochrones of various metallicities), so our choice of metallicity has no bearing on the derived distance modulus.

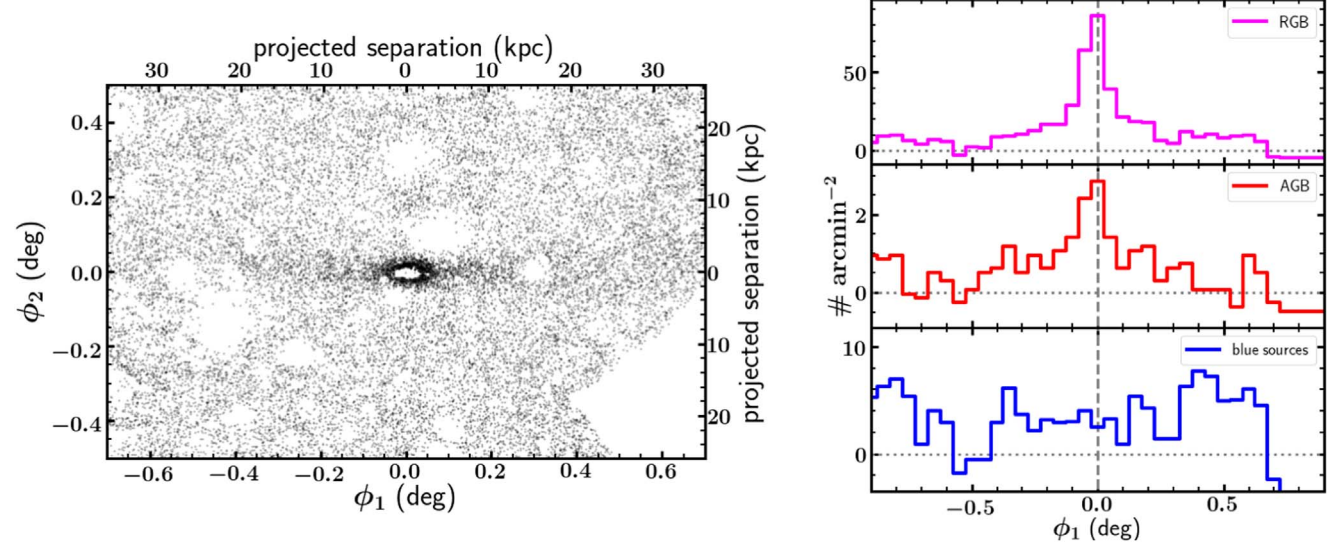


Figure 5. Left panel: scatter plot showing positions (in coordinates aligned with the DDO 44 stream) of RGB candidate stars, showing the clear detection of the stream as an overdensity. The upper and right axes show the projected separation in kpc assuming a distance of 2.96 Mpc (Section 3.1). Empty circular regions are "halos" around bright stars where the detection algorithm flags sources as unreliable. Right panel: number density of sources along the stream in a strip within $\phi_2 = \pm 0^{\circ}05$. From top to bottom, the panels show sources selected using the polygons in Figure 4 to highlight RGB stars (top panel), AGB stars (middle panel), and blue sources (bottom panel). In each panel, we have subtracted off the mean background in surrounding regions that are free from "holes" due to bright stars. There is a peak in the AGB profile at $\phi_1 \sim 0^{\circ}$ corresponding to the RGB peak. In the lower panel, no corresponding peak is seen among the blue sources, suggesting that these are unresolved background galaxies rather than young stars associated with DDO 44.

minimization based on differences between the DDO 44 stellar sample and the isochrones to find a best-fitting metallicity of $[Fe/H]=-1.6\pm0.3$. This mean metallicity is consistent with those measured by (Karachentsev et al. 1999, -1.7 ± 0.4), (Alonso-García et al. 2006, -1.54 ± 0.14), and (Lianou et al. 2010, -1.67 ± 0.19) via HST imaging. Figure 4 shows a CMD of the central 2-4' field around DDO 44, with the best-fit isochrone at [Fe/H]=-1.6 overlaid, along with isochrones at ±0.5 dex in metallicity.

The RGB of DDO 44 is wider than expected solely based on photometric errors. This could be due in part to photometric scatter induced by the significant unresolved emission in the body of DDO 44. However, Alonso-García et al. (2006) estimated that as much as 20% of the total stellar content of DDO 44 is contributed by the intermediate-age population (likewise, Lianou et al. 2010 found the fraction of AGB stars relative to RGB number to be $f_{AGB} = 0.11$). Thus, a single 10 Gyr population should not be expected to reproduce the width of the RGB. Estimating the relative contributions of the different age populations (i.e., a star formation history (SFH)) is beyond the scope of the current study (and is typically best achieved with data reaching the oldest MSTO). Finally, we note that we calculated a metallicity distribution under the assumption that only 10 Gyr populations were present (assigning stellar metallicities based on isochrones), and found a metallicity spread of ~ 0.49 dex (determined by fitting a Gaussian to the distribution). The mean metallicity and metallicity spread (with the caveat that we have assumed a single age) is similar to those of MW dSphs with similar luminosities (e.g., the Sculptor dSph; Simon 2019), suggesting that some of the RGB width is contributed by a metallicity spread in DDO 44, while the presence of intermediate-age populations may account for some additional broadening of the RGB.

Based on the lack of blue stars in *HST* images of DDO 44, Karachentsev et al. (1999) estimated that the most recent star

formation in DDO 44 was at least 300 Myr ago. We do not see evidence of this young population beyond 2'. However, a significant population of bright AGB stars above the TRGB (also seen in HST data by Karachentsev et al. 1999 and Alonso-García et al. 2006) suggests that intermediate-age populations are present in the outer regions of DDO 44. Indeed, as noted previously, Alonso-García et al. (2006) found that \sim 20% of the stellar population of DDO 44 consists of intermediate-age (between \sim 5–8 Gyr, and at least older than 2 Gyr) populations.

3.2. Stellar Populations in the Stream

To facilitate analysis of the stream, we first derived the transformation to a coordinate system aligned with the stream. We determined the central position at points along the stream by fitting Gaussians to the stellar density in slices of 0°.1 in decl. Using the two points immediately adjacent to DDO 44, but on the north and south sides, we derived the transformation to a great circle coordinate frame using the gala 16 software. This transformation places DDO 44 at the origin, with angle ϕ_1 along the stream, and ϕ_2 perpendicular to the stream. A map of RGB stars in the transformed coordinates is shown in the left panel of Figure 5.

We then selected narrow strips of $|\phi_2| < 0.05$, and extracted an RGB star density profile as a function of ϕ_1 (i.e., along the stream). This profile is shown in the right panel of Figure 5, where we have subtracted the mean density in background regions that do not contain bright star holes (seen as white voids in Figure 5). The three background regions are at -0.05 (seen as white voids in Figure 5). The three background regions are at -0.05 (seen as white voids in Figure 5). The three background regions are at -0.05 (seen as white voids in Figure 5). The three background regions are at -0.05 (seen as white voids in Figure 5). The three background regions are at -0.05 (seen as white voids in Figure 5). The three background regions are at -0.05 (seen as white voids in Figure 5). The three background regions are at -0.05 (seen as white voids in Figure 5). The three background regions are at -0.05 (seen as white voids in Figure 5). The three background regions are at -0.05 (seen as white voids in Figure 5). The three background regions are at -0.05 (seen as white voids in Figure 5). The three background regions are at -0.05 (seen as white voids in Figure 5). The three background regions are at -0.05 (seen as white voids in Figure 5). The three background regions are at -0.05 (seen as white voids in Figure 5).

¹⁶ http://gala.adrian.pw/en/latest/

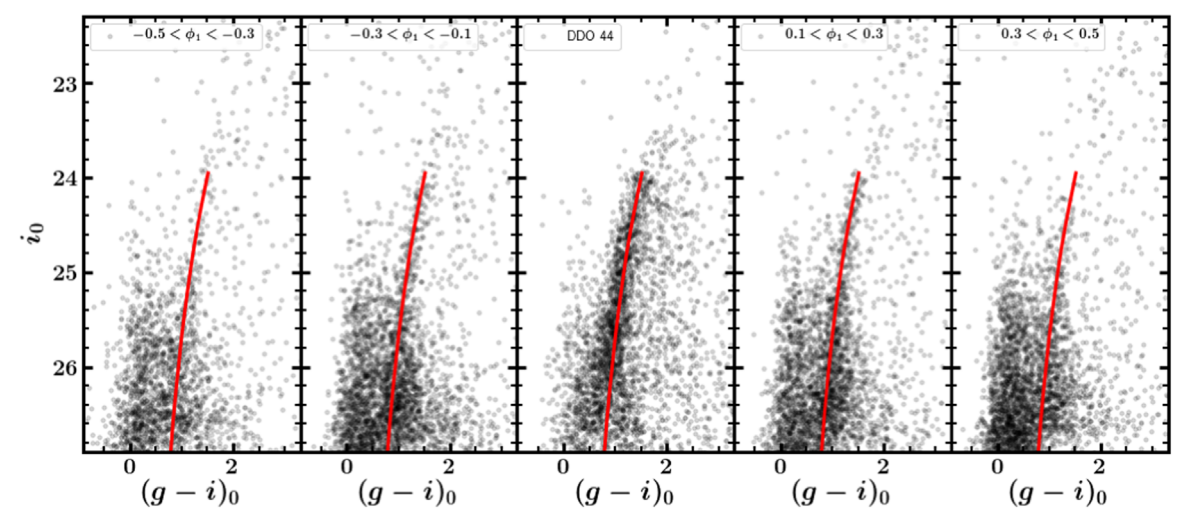


Figure 6. CMDs selected in angular bins along the stream, within $|\phi_2| < 0.05$ of the stream center. The isochrone is the same [Fe/H] = -1.6 isochrone used in Figure 4. Stellar populations consistent with DDO 44 are seen to at least $|\phi_1| = 0.3$ (~ 16 kpc at the distance of DDO 44), and perhaps as far as $|\phi_1| = 0.5$ (~ 26 kpc at the distance of DDO 44) from DDO 44.

Figure 6 highlights CMDs of stars extracted in bins along the stream. The central panel contains the core of DDO 44 (within 0.1), with panels to the left (south) and right (north) showing similar stellar populations extending into the stream. On both sides of DDO 44, the stream is barely noticeable (if at all) at $|\phi_1| \gtrsim 0$ °.4. The best-fit isochrone with [Fe/H] = -1.6 is a good match to the RGB stellar populations in both the core and stream. The bright AGB stars visible in the central regions of DDO 44 are seen in small numbers at all radii (and indeed, the density profile seen in Figure 5 suggests that the AGB stars extend as far as the RGB stars in the stream). The fact that the oldest RGB stars and the intermediate-age AGB populations are both extended suggests that DDO 44 had little to no population gradient in its core before being tidally disrupted (however, Lianou et al. 2010 found that metal-rich populations are more centrally concentrated in DDO 44 than metal-poor stars).

3.3. Total Luminosity

To estimate the total luminosity of DDO 44, including stars in its streams, we summed the flux of all RGB stars brighter than $i_0 < 26.5$, applying a completeness correction to each star's flux based on the fits in Figure 2. We then corrected for the unmeasured luminosity below the cutoff magnitude using a Dartmouth isochrone (Dotter et al. 2008) with [Fe/H] = -1.6, 10 Gyr age, and power-law luminosity function slope of -1.5.¹⁷ From this luminosity function, we determine that \sim 22% of the flux is in stars brighter than i = 26.5; we thus apply a correction to the total flux to account for the remaining 78% of the light. Finally, we account for the "missing" data due to stellar crowding near the center of DDO 44 by excluding the inner 2' from our calculations. Adopting $\mu_{R,0} = 24.1$ mag arcsec⁻² and a scale length of 39" (Karachentsev et al. 1999), we estimate that $\sim 60\%$ of the light is contained within our excluded 2' region.

We find $M_{i,\text{tot}} = -13.4$ and $M_{g,\text{tot}} = -12.6$ for the total luminosity of DDO 44 and the stars in its streams, where we take the region between $|\phi_1| < 0.1$ to be the main body of

DDO 44. Of the total, $\sim 17\%$ and $\sim 11\%$ of the flux are contained in the northern (0.1 < ϕ_1 < 0.7) and southern $(-0.7 < \phi_1 < -0.1)$ portions of the stream, respectively. Given the many large corrections detailed in the previous paragraph, it is difficult to place uncertainties on these estimates. To facilitate comparison to the measurement by Karachentsev et al. (1999) of $M_R = -13.1$, we transform these absolute magnitudes in the PanSTARRS system to the Johnson-Cousins R-band using the relations from Table 6 of Tonry et al. (2012). This yields a total $M_R \sim -13.3$ based on our HSC measurements. Removing the \sim 20%-30% of the resolved stars' flux that we find beyond 6' of the DDO 44 center would reduce our derived luminosity of DDO 44 by \sim 0.2–0.3 mag, placing our estimate for the central body of the galaxy in excellent agreement with that of Karachentsev et al. (1999).

To make connections with theory, it is useful to translate from the object's absolute magnitude to stellar mass. Our measured luminosity transforms to $M_V = -12.9$ (it is Local Group convention to report V-band absolute magnitudes), which corresponds to $M_* = 2.0 \times 10^7 \, M_\odot$ (assuming a V-band stellar mass $(M/L)_V$ of 1.6; Woo et al. 2008). Note that an estimate based on the K-band luminosity from Karachentsev et al. (2013), assuming $(M/L)_K = 1$, gives $M_* = 6.0 \times 10^7 \, M_\odot$ for DDO 44.

By fitting Gaussians to the resolved stellar surface density along the major and minor axes, we find an ellipticity $\epsilon \equiv 1 - b/a \approx 0.6$. It is unsurprising that DDO 44 is rather extended, and that its ellipticity is similar to that of the tidally disrupting Sagittarius dSph ($\epsilon = 0.64$; McConnachie 2012). Also, like the Sagittarius dSph, DDO 44's surface brightness (as measured by Jerjen et al. 2001) lies below that of typical dwarfs at its luminosity (see, e.g., Figure 7 from McConnachie 2012), as expected for a system undergoing tidal disruption. DDO 44's closest analogs in luminosity and stellar mass are, according to McConnachie (2012), Sagittarius $(M_V = -13.5)$, Fornax $(M_V = -13.4)$, and And VII $(M_V = -12.6)$. Of these three, only Sagittarius is clearly disrupting—deep imaging data show no hints of tidal features for Fornax (Wang et al. 2019), and the ellipticities of Fornax and And VII are far lower. Our derived metallicity for DDO 44

 $[\]overline{^{17}}$ Note that if instead we use a Salpeter IMF, our derived total luminosity of DDO 44 changes by <0.03 mag

Table 1Properties of DDO 44 and Its Stream

Parameter	Value	Reference
R.A.	07:34:11.50	NED
Decl.	+66:52:47.0	NED
m-M	27.36 ± 0.07	this work
D (Mpc)	2.96 ± 0.10	this work
M_V	-12.9	this work
$M_* (M_{\odot})$	2×10^{7}	this work
[Fe/H]	-1.6 ± 0.3	this work
Ellipticity	0.6	this work
R _e (kpc)	0.74 ± 0.02	Jerjen et al. (2001)
$<\mu_e>$ (B)	26.00	Jerjen et al. (2001)
H I mass (M_{\odot})	$< 10^{6}$	KK07 ^a
stream extent (°)	~1°	this work
stream extent (kpc)	~50	this work
$L_{\rm stream}/L_{\rm tot}^{b}$	\sim 20% $-$ 30%	this work

Notes.

of [Fe/H] = -1.6 is near, but slightly on the low metallicity side of the luminosity-metallicity relation for Local Group dwarf galaxies (e.g., McConnachie 2012; Kirby et al. 2013). The metallicities of Sagittarius, Fornax, and And VII are all significantly higher (Kalirai et al. 2010; Kirby et al. 2011; Carlin et al. 2012; McConnachie 2012; Hasselquist et al. 2019).

We summarize the properties of DDO 44 and its stream in Table 1, including some relevant data from the literature.

4. DDO 44 and Its Streams in Context

DDO 44 is clearly a disrupting dwarf, but questions remain about its history and association with a larger host. In this section, we argue that NGC 2403 is the most likely host for DDO 44. This conclusion allows us to use simulations to estimate how rare (or not) it is for a large dwarf to be disrupting around a low-mass host, and consider how the orbit of DDO 44 explains various features of its SFH. We may also place DDO 44 in the context of the NGC 2403 satellite system, and consider whether NGC 2403's satellite luminosity function is in line with expectations from the ΛCDM paradigm.

4.1. DDO 44 Is a Satellite of NGC 2403

We consider whether DDO 44 is in fact a satellite of NGC 2403 or of the neighboring galaxy NGC 2366.

DDO 44 has a heliocentric radial velocity of $213 \, \mathrm{km \, s^{-1}}$ (Karachentsev et al. 2011; Tully et al. 2016), ¹⁸ while the Tully et al. "COSMICFLOWS-3" catalog gives $v_{hel} = 141 \, \mathrm{km \, s^{-1}}$ for NGC 2403. This small difference in their relative velocities (for context, this velocity difference of $\sim 70 \, \mathrm{km \, s^{-1}}$ is much less than the escape velocity from NGC 2403 of $\gtrsim 200 \, \mathrm{km \, s^{-1}}$; see Figure 7), in addition to the nearly identical distance moduli of DDO 44 and NGC 2403 (Section 3.1) is suggestive of an association between the two galaxies.

We also note that the extension of the DDO 44 stream points in the general direction of nearby, roughly SMC stellar mass,

galaxy NGC 2366 ($D \sim 3.3$ Mpc; Karachentsev et al. 2013), which is $\sim 2^{\circ}.4$ north (position angle 348° east of north) of DDO 44. In spite of the fact DDO 44's projected distance from NGC 2366 of \sim 130 kpc is likely beyond the virial radius of NGC 2366 ($R_{\rm vir} \sim 110 \, \rm kpc$ for a slightly sub-SMC stellar-mass galaxy; e.g., Dooley et al. 2017), it is interesting to note that its radial velocity of 103 km s⁻¹ is similar to the 213 km s⁻¹ velocity of DDO 44 (i.e., the difference of $\sim 110 \,\mathrm{km \, s^{-1}}$ is likely less than the escape velocity of NGC 2366). NGC 2366 is actively star-forming, with distortions in its HI contours (Lelli et al. 2014), indicating a recent interaction (which Lelli et al. attributed to an ongoing minor merger with NGC 2363). We believe it is unlikely that NGC 2366 caused the visible damage to DDO 44. NGC 2366 is a gas-rich dwarf galaxy, with ordered rotation and a rotation velocity of only \sim 60 km s⁻¹ (Oh et al. 2008). Only a small fraction of its H I layer is discrepant from the otherwise well-behaved rotation. In order to feel significant tidal effects, DDO 44 would have needed to pass very near NGC 2366, in which case NGC 2366 would have felt strong tidal forces in this \sim 25:1 stellar massratio interaction (examples of similar mass-ratio interactions in the Local Volume can be seen in Pearson et al. 2016). It thus seems implausible that a galaxy as small as NGC 2366 has stripped away all the gas, \sim 90% of the dark matter, and \sim 25% of the stars in DDO 44.

In summary, many pieces of evidence make it more likely that DDO 44 interacted with the more massive NGC 2403 than its less massive neighbor NGC 2366: (1) DDO 44 is closer to NGC 2403 in projected and line-of-sight separation than it is to NGC 2366, (2) DDO 44 is likely beyond the virial radius of NGC 2366 (and within that of NGC 2403), (3) DDO 44's velocity is closer to that of NGC 2403 than to NGC 2366, (4) this relative velocity is less than the expected escape velocity of NGC 2403, and (5) NGC 2403 is more massive than NGC 2366, and thus more likely to host (and retain) a large dSph such as DDO 44.

4.2. DDO 44 Has an Unusual Orbit about Its Host

In order to investigate how common disrupted satellites like DDO 44 are around galaxies like NGC 2403, we search for analog systems in cosmological simulations. If analog systems are common, we can use the present-day kinematics of the DDO 44 analogs to estimate pericenter and apocenter distributions and use merger trees to track their orbital histories, giving us insight into the interaction history of the system. If very few analog systems are identified, then we can infer that the DDO 44-NGC 2403 system is, in some way, an extreme interaction. We may also use the infall time distribution function and the orbital history to constrain models for the physical origin of the truncation of DDO 44's SFH. This analysis is based in part on work by Rocha et al. (2012), and is similar to the approach taken by Besla et al. (2018). A full description is found in Garling et al. (2019), but a brief description is given below.

We use the Illustris simulations (Vogelsberger et al. 2013, 2014a, 2014b; Genel et al. 2014; Nelson et al. 2015; Rodriguez-Gomez et al. 2015) for this analysis. Illustris is simulated with WMAP9 Λ CDM cosmological parameters (Hinshaw et al. 2013). We use the flagship Illustris-1 run, which simulates a comoving box of volume 106.5 Mpc³ with 1820^3 particles each of dark matter, gas, and tracers that are used to track the Lagrangian evolution of the gas (Genel et al.

^a Karachentsev & Kaisin (2007).

^b Fraction of luminosity in the stream.

¹⁸ Note that this velocity is apparently based solely on a HII region offset from the center of DDO 44, but likely associated with it. We could not locate any extant velocity measurements based on the stellar body of DDO 44.

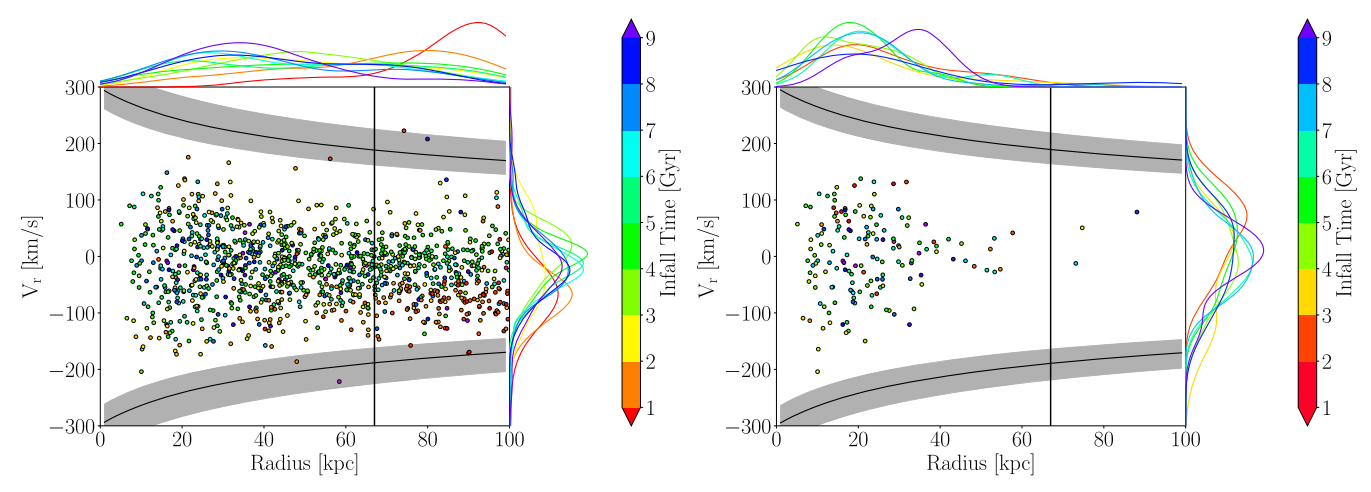


Figure 7. Left panel: distribution of DDO 44 analogs from Illustris-1 in radial velocity and radius (relative to their host), without the tidal disruption criterion applied. Typical escape velocity curves are overplotted, and the projected distance of DDO 44 from NGC 2403 (67 kpc) is shown with a solid line. Illustris-1 analogs are color-coded according to infall time, with the most recent infalls labeled in red and the earliest infalls labeled purple. The relative host-subhalo radial velocity (left) and separation (top) probability distribution functions are given as a function of infall time. Right panel: same as left, but with the tidal disruption criterion of $M_{z=0}/M_{infall} \le 0.1$ applied. This population consists of primarily early accretions that have made several orbits, and only three systems have 3D radii that are greater than DDO 44's projected radius.

2013). We replicate our analysis on the Illustris-1-Dark run, which simulates the same volume as Illustris-1 with the same number of dark matter particles but without hydrodynamics, and find no significant differences from the analysis presented below for Illustris-1. We utilize the friends-of-friends group catalogs, SUBFIND subhalo catalogs, and the SUBLINK merger trees (Rodriguez-Gomez et al. 2015) to identify halos and subhalos and track their evolution through time.

Because the hydrodynamic mass resolution is too low for us to identify analog systems using the simulated stellar masses, we instead find analog systems based on dark-matter halo masses and abundance matching. We identify analog systems in Illustris by matching SUBFIND subhalo masses to halo masses for DDO 44 and NGC 2403, calculated by converting their stellar masses to halo masses using the abundance matching scheme of Moster et al. (2013), which returns halo masses of $2.8 \times 10^{10} M_{\odot}$ and $2.5 \times 10^{11} M_{\odot}$ for DDO 44 and NGC 2403, respectively.

In searching for analog systems, we require that NGC 2403 analogs be the most massive subhalo in their group (i.e., the host) and DDO 44 analogs be the second-most massive subhalo in the group (i.e., most massive satellite). To take into account scatter in the stellar-to-halo-mass relation and the uncertainty in stellar mass, we accept systems that have masses within a factor of two of the above halo masses. For the DDO 44 analogs, we place this mass constraint on first infall mass rather than present-day mass, as the majority of a satellite's stellar mass is typically formed prior to accretion by its present-day host (i.e., when it was a central galaxy of its own), and we expect mass loss to be significant for true DDO 44 analogs. We define first infall as the time when DDO 44 analogs first enter the virial radius of their present-day NGC 2403 analog hosts.

Given that DDO 44's stellar population is disrupted, we can infer that its dark matter halo is as well. Because dwarf stellar populations are deeply embedded within their dark matter halos, the degree of disruption to the dark matter halo must be severe—Peñarrubia et al. (2008) showed that King profiles embedded in Navarro–Frenk–White halos must have $\sim 90\%$ of their dark matter halo stripped before stars begin to be disrupted. This criterion is valid regardless of whether the

subhalo is cored or cusped, as differences in tidal stripping between the two density profiles only become important when the tidal radius approaches the size of the core, which typically has an enclosed mass less than 10% of the infall halo mass (Dooley et al. 2016; Garrison-Kimmel et al. 2017). As such, we place an additional disruption criterion on our DDO 44 analogs and only accept systems with $M_{z=0}/M_{\rm infall} \leq 0.1$. This proves to be a very strong condition, as shown in Figure 7. There are 1628 undisrupted analog systems, but only 157 systems remain when the disruption criterion is imposed. 19 These remaining systems have predominantly early infall times (mean ~ 7 Gyr), have made several complete orbits with present-day mean eccentricity ~ 0.5 , and have small apocenters of 30–70 kpc; we interpret the majority of this population to represent satellites that were accreted early and lost mass gradually. Given DDO 44's projected distance of 67 kpc (and thus likely a much larger apocenter), we do not believe this population is representative of DDO 44.

Next we discuss the three systems with radii greater than $67 \,\mathrm{kpc}$, shown to the right of the line in Figure 7. Two of these systems have relatively early infall times (7–9 Gyr). These systems have much larger apocenters than is typical for other satellites in the population with similar infall times (>150 kpc compared to 30–70 kpc). We attribute this to their more eccentric orbits (e > 0.7 at present day) which allow them to maintain low binding energies over many orbits due to the lessened effects of dynamical friction compared to the bulk of the population. For reasons associated with the SFH and the morphology of NGC 2403's gas (described in Section 4.3), we consider these orbits unlikely.

Most interesting is the subhalo identified with an infall time \sim 3.5 Gyr and an apocenter of \sim 150 kpc, much larger than DDO 44's projected distance of 67 kpc. This subhalo has an orbital eccentricity greater than 0.8 at present day, and has lost more than 90% of its mass over only a handful of orbits. Such a

¹⁹ Note that systems for which the halo finder does not identify a subhalo remnant are not included in this count. Systems that may be missed by the halo finder include satellites that are fully disrupted or where the remaining mass lies below the resolution limit of the simulation, or where a stripped subhalo lies close to the host halo center even if the subhalo is not fully disrupted.

configuration, with a highly radial orbit, would be highly effective at stripping the dark matter halo sufficiently to disrupt the stellar population.

In summary, we find that DDO 44's existence is rare for a host galaxy like NGC 2403. Limiting our simulated sample to NGC 2403-mass analogs with DDO 44-mass analog satellites, we find that only $\sim 0.1\%$ of these analogs have a disrupting DDO 44 with a large separation between host and satellite. About 10% of analogs are disrupting but are located much closer to the host. We argue that DDO 44 is likely a recently accreted satellite with a highly eccentric orbit.

4.3. Insights from DDO 44's Orbit on Its SFH

We now combine the orbital information from the previous section with DDO 44's current gas content and measured SFH to estimate a timescale and identify the physical process likely to be responsible for the end of star formation in this galaxy.

The SFH of DDO 44 (Girardi et al. 2010; Weisz et al. 2011) suggests that it formed $\sim 15\%-20\%$ of its stars between 1 and 3 Gyr ago. However, Karachentsev & Kaisin (2007) found an upper limit on the neutral hydrogen content of DDO 44 of only $M_{\rm H\,I} < 10^6 \, M_{\odot}$, and no H α emission associated with DDO 44. Given that it has no hint of gas, this star formation event (and/or the interaction leading to the tidal features) must have exhausted whatever neutral hydrogen DDO 44 still had.

In this regard, it is interesting to note that de Blok et al. (2014) suggested that a flyby encounter between NGC 2403 and DDO 44 could be responsible for the anomalous cloud of HI detected at the northwest edge of the NGC 2403 disk. In their Figure 8, de Blok et al. (2014) overlay the contours of this H I cloud on a map of RGB stars from Barker et al. (2012), showing a disturbance in the outer stellar disk (also visible in our RGB density map in Figure 3) at the location of the HI cloud, roughly in the direction of the DDO 44 stream's projected intersection with the NGC 2403 disk. The H I cloud has a mass of $\sim 6 \times 10^6 M_{\odot}$. This is within roughly an order of magnitude of the stellar mass of DDO 44, so it is plausible that the H_I cloud is material stripped from DDO 44 (though we note that the gas could also have been pulled from NGC 2403 during the interaction). Interestingly, Lianou et al. (2010) found that DDO 44 lies in the "transition region" in luminositymetallicity space between the locations occupied by dSphs (i.e., typically quenched systems) and dIrrs (typically gas-rich, starforming systems). Unlike the three other M81-group dSphs found by Lianou et al. to reside in this transition region, DDO 44 does not have H I or H α , suggesting that its gas may have been removed recently.

A recent infall is potentially also supported by the SFH of NGC 2403. We note that there was also a slight upturn in the SFH of NGC 2403 within the past ~2 Gyr (Williams et al. 2013), which possibly could have arisen due to an interaction with a satellite such as DDO 44. We do note, however, that in the same study based on deep *HST+ACS* observations (Williams et al. 2013), it is claimed that the disk of NGC 2403 appears "remarkably undisturbed." Refined spectroscopic measurements of the velocity of DDO 44 (based on the

stellar light rather than the lone H II region) may enable modeling of its orbit that can reconcile the apparently conflicting information given by the H I and the stellar disk of NGC 2403.

These lines of evidence suggest a recent (1–2 Gyr ago) close interaction between DDO 44 and NGC 2403 that tidally stripped DDO 44's H I reservoir. The travel time between the small pericenter and DDO 44's current position with respect to NGC 2403 is approximately 1 Gyr. Because the gas scale length generically exceeds the optical size of galaxies, stellar stripping is a sign that gas ought to have been heavily tidally stripped as well (Leisman et al. 2017). While it is possible that gas may have additionally been ram-pressure-stripped from DDO 44, the small pericenter implied by the H I distribution and SFH of NGC 2403 suggests tides play the dominant role in removing gas and quenching star formation in DDO 44.

In short, the SFH suggests a relatively recent infall for DDO 44, on a highly unusual orbit, for which much of the cold gas fuel for star formation was tidally stripped during the last pericenter passage.

4.4. NGC 2403's Satellite Luminosity Function

We place DDO 44 in the context of its role as the most massive satellite of NGC 2403. DDO 44 is one of two known satellites of NGC 2403, and is by far the most massive. The stellar mass ratio between NGC 2403 ($M_* \sim 7 \times 10^9 M_{\odot}$) and DDO 44 is ~ 350 (i.e., a stellar mass gap of $\Delta M_* = \log(M_{\rm N2403}/M_{\rm max,sat}) \sim 2.5$). Because of the steepness of the halo mass function and the stellar-mass-halo-mass relation, this mass ratio is not unusual. According to the analysis of satellite galaxies in the Sloan Digital Sky Survey (York et al. 2000) by Sales et al. (2013), we expect there to be approximately one satellite with a stellar mass exceeding 0.1% of the host's stellar mass in the virial volume of NGC 2403. However, the mass gap between NGC 2403's first- and secondmost-massive satellite is unusual. The gap between the stellar masses of DDO 44 and second-most-massive NGC 2403 satellite (MADCASH J074238+652501-dw; Carlin et al. 2016; $M_* \sim 1 \times 10^5 M_{\odot}$) is a factor of ~ 200 . Based on predictions from models (Dooley et al. 2017; see also Jahn et al. 2019 for predictions from the FIRE simulations), we expect that NGC 2403 should host between 2 and 8 satellites with stellar masses $> 10^5 M_{\odot}$ (the uncertainty arises both from halo-to-halo variation and the as-yet poorly constrained stellar-mass-halomass relation on these scales), so the observation of only one satellite below DDO 44's stellar mass down to $M_* \sim 10^5 M_{\odot}$ is unusual in both the size of the gap and the total number of

While a systematic search and characterization of our completeness will be the subject of a future contribution, the fact that we only find two companions to NGC 2403 in our preliminary search implies that this LMC analog may be lacking bright satellites (relative to predictions).

5. Discussion and Conclusions

We report the discovery of a stellar tidal stream around the Local Volume dwarf spheroidal galaxy DDO 44, based on deep, resolved-star observations with Subaru+HSC. The tidal stream stretches ~ 25 kpc on either side of the main body of DDO 44, and is oriented toward NGC 2403, of which DDO 44 is likely a satellite. We reconstruct the total luminosity of the

 $[\]overline{^{20}}$ Note that Karachentsev et al. (2011) found evidence of a small (\sim 4" in size), off-center H II region possibly associated with DDO 44, with H α emission and possibly some late B-type stars associated with it. Karachentsev et al. (2011) suggest that this small bit of star formation is in a clump of accreted intergalactic gas. It is also possible that it was picked up during DDO 44's recent interaction with NGC 2403.

DDO 44 progenitor, and find that it had a luminosity of at least $M_{i,\text{tot}} = -13.4$ ($M_{g,\text{tot}} = -12.6$; or $M_{V,\text{tot}} = -12.9$).

Using the Illustris simulation suite, we show that DDO 44 is an unusual object. While disruptions by LMC-mass hosts are not uncommon (10% of our mass-matched analog systems show a massive disrupting dwarf), and observed in other LMC analog systems (notably NGC 4449; Karachentsev et al. 2007; Martínez-Delgado et al. 2012; Rich et al. 2012; Toloba et al. 2016), the typical separation with respect to the host in Illustris is much smaller than what is observed for the NGC 2403-DDO 44 system. We find only $\sim 0.1\%$ of our mass-matched analog systems are disrupting with the type of large observed separation between NGC 2403 and DDO 44. Combined with observations of the H I distribution of both galaxies, the recent upturn of star formation in NGC 2403, and the recent quenching of DDO 44, we argue that DDO 44 only recently entered the halo of NGC 2403 on a high-eccentricity orbit with a pericenter small enough to tidally strip both its stars and its gas reservoir.

This work strengthens the case for significant interaction in dwarf pairs, even for dwarf systems with high mass ratios (~ 100) like the NGC 2403-DDO 44 system. NGC 2403's recent upturn in star formation rate is consistent with our estimated infall and pericenter passage of DDO 44. The TiNy Titans survey found that starbursts are more frequent for dwarf pairs than for field dwarfs, although they included systems with much lower mass ratios than we consider in this study (Stierwalt et al. 2015). Furthermore, the quenching and obvious tidal stripping of DDO 44 shows that even low-mass hosts may exert considerable environmental influence over their satellites. Although a systematic analysis of the strength and prevalence of environmental quenching of satellite galaxies by LMC-like hosts is beyond the scope of this work, we a have presented evidence that even low-mass hosts can quickly quench and destroy massive satellites.

We thank the referee for insightful comments that helped clarify this work. We acknowledge support from the following NSF grants: AST-1816196 (J.L.C.); AST-1814208 (D.C.); AST-1813628 (A.H.G.P. and C.T.G.); and AST-1616710 (A.J. R.). A.J.R. was supported as a Research Corporation for Science Advancement Cottrell Scholar. J.S. acknowledges support from the Packard Foundation. Research by D.J.S. is supported by NSF grants AST-1821987, AST-1821967, AST-1813708, and AST-1813466. The work of authors J.L.C., D.J. S., and J.R.H. was performed in part at the Aspen Center for Physics, which is supported by National Science Foundation grant PHY-1607611.

This research has made use of NASA's Astrophysics Data System, and Astropy, a community-developed core Python package for Astronomy (Price-Whelan et al. 2018).

The Pan-STARRS1 Surveys have been made possible through contributions of the Institute for Astronomy, the University of Hawaii, the PanSTARRS Project Office, the Max-Planck Society and its participating institutes, the Max Planck Institute for Astronomy, Heidelberg and the Max Planck Institute for Extraterrestrial Physics, Garching, The Johns Hopkins University, Durham University, the University of Edinburgh, Queen's University Belfast, the Harvard-Smithsonian Center for Astrophysics, the Las Cumbres Observatory Global Telescope Network Incorporated, the National Central University of Taiwan, the Space Telescope

Science Institute, the National Aeronautics and Space Administration under grant No. NNX08AR22G issued through the Planetary Science Division of the NASA Science Mission Directorate, the National Science Foundation under grant AST-1238877, the University of Maryland, Eotvos Lorand University (ELTE), and the Los Alamos National Laboratory.

Facilities: Subaru+HSC, PS1.

Software: astropy (Robitaille et al. 2013; Price-Whelan et al. 2018), gala (Price-Whelan 2017), Matplotlib (Hunter 2007), NumPy (van der Walt et al. 2011), Topcat (Taylor 2005).

ORCID iDs

Jeffrey L. Carlin https://orcid.org/0000-0002-3936-9628 Christopher T. Garling https://orcid.org/0000-0001-9061-1697

Annika H. G. Peter https://orcid.org/0000-0002-8040-6785 Denija Crnojević https://orcid.org/0000-0002-1763-4128 Jonathan R. Hargis https://orcid.org/0000-0002-8722-9806 Burçin Mutlu-Pakdil https://orcid.org/0000-0001-9649-4815

Ragadeepika Pucha https://orcid.org/0000-0002-4940-3009 Aaron J. Romanowsky https://orcid.org/0000-0003-2473-0369

David J. Sand https://orcid.org/0000-0003-4102-380X Kristine Spekkens https://orcid.org/0000-0002-0956-7949 Jay Strader https://orcid.org/0000-0002-1468-9668 Beth Willman https://orcid.org/0000-0003-2892-9906

References

```
Aihara, H., Arimoto, N., Armstrong, R., et al. 2018a, PASJ, 70, S4
Aihara, H., Armstrong, R., Bickerton, S., et al. 2018b, PASJ, 70, S8
Alonso-García, J., Mateo, M., & Aparicio, A. 2006, PASP, 118, 580
Barkana, R., & Loeb, A. 1999, ApJ, 523, 54
Barker, M. K., Ferguson, A. M. N., Irwin, M. J., et al. 2012, MNRAS,
   419, 1489
Belokurov, V., Zucker, D., Evans, N., et al. 2006, ApJL, 642, L137
Belokurov, V., Zucker, D., Evans, N., et al. 2007, ApJ, 654, 897
Bennet, P., Sand, D. J., Crnojević, D., et al. 2017, ApJ, 850, 109
Bennet, P., Sand, D. J., Crnojević, D., et al. 2019, arXiv:1906.03230
Bennet, P., Sand, D. J., Zaritsky, D., et al. 2018, ApJL, 866, L11
Benson, A. J., Frenk, C. S., Lacey, C. G., Baugh, C. M., & Cole, S. 2002,
   MNRAS, 333, 177
Besla, G., Patton, D. R., Stierwalt, S., et al. 2018, MNRAS, 480, 3376
Birnboim, Y., & Dekel, A. 2003, MNRAS, 345, 349
Bordoloi, R., Tumlinson, J., Werk, J. K., et al. 2014, ApJ, 796, 136
Bosch, J., Armstrong, R., Bickerton, S., et al. 2018, PASJ, 70, S5
Bose, S., Deason, A. J., & Frenk, C. S. 2018, ApJ, 863, 123
Brooks, A. M., Governato, F., Quinn, T., Brook, C. B., & Wadsley, J. 2009,
   ApJ, 694, 396
Brown, T. M., Tumlinson, J., Geha, M., et al. 2014, ApJ, 796, 91
Carlin, J. L., Sand, D. J., Price, P., et al. 2016, ApJL, 828, L5
Carlin, J. L., Yam, W., Casetti-Dinescu, D. I., et al. 2012, ApJ, 753, 145
Chiboucas, K., Jacobs, B. A., Tully, R. B., & Karachentsev, I. D. 2013, AJ,
Choi, J., Dotter, A., Conroy, C., et al. 2016, ApJ, 823, 102
Crnojević, D., Sand, D. J., Bennet, P., et al. 2019, ApJ, 872, 80
Dalcanton, J. J., Williams, B. F., Seth, A. C., et al. 2009, ApJS, 183, 67
Danieli, S., van Dokkum, P., & Conroy, C. 2017, ApJ, 856, 69
de Blok, W. J. G., Keating, K. M., Pisano, D. J., et al. 2014, A&A, 569, A68
Dekel, A., & Birnboim, Y. 2006, MNRAS, 368, 2
Dooley, G. A., Peter, A. H. G., Carlin, J. L., et al. 2017, MNRAS, 472, 1060
Dooley, G. A., Peter, A. H. G., Vogelsberger, M., et al. 2016, MNRAS,
   461, 710
Dotter, A. 2016, ApJS, 222, 8
Dotter, A., Chaboyer, B., Jevremović, D., et al. 2008, ApJS, 178, 89
Drlica-Wagner, A., Bechtol, K., Allam, S., et al. 2016, ApJL, 833, L5
Drlica-Wagner, A., Bechtol, K., Rykoff, E. S., et al. 2015, ApJ, 813, 109
```

```
Fielding, D., Quataert, E., McCourt, M., & Thompson, T. A. 2017, MNRAS,
Fillingham, S. P., Cooper, M. C., Pace, A. B., et al. 2016, MNRAS, 463, 1916
Fillingham, S. P., Cooper, M. C., Wheeler, C., et al. 2015, MNRAS, 454, 2039
Fraternali, F., & Binney, J. J. 2006, MNRAS, 366, 449
Fraternali, F., van Moorsel, G., Sancisi, R., & Oosterloo, T. 2002, AJ,
   123, 3124
Furusawa, H., Koike, M., Takata, T., et al. 2018, PASJ, 70, S3
Garling, C. T., Peter, A. H. G., Kochanek, C. S., et al. 2019, arXiv:1908.11367
Garrison-Kimmel, S., Wetzel, A., Bullock, J. S., et al. 2017, MNRAS,
Genel, S., Vogelsberger, M., Nelson, D., et al. 2013, MNRAS, 435, 1426
Genel, S., Vogelsberger, M., Springel, V., et al. 2014, MNRAS, 445, 175
Girardi, L., Williams, B. F., Gilbert, K. M., et al. 2010, ApJ, 724, 1030
Grcevich, J., & Putman, M. E. 2009, ApJ, 696, 385
Grillmair, C. J., & Carlin, J. L. 2016, in Tidal Streams in the Local Group and
  Beyond, ed. H. J. Newberg & J. L. Carlin, 420 (Berlin: Springer), 87
Hafen, Z., Faucher-Giguère, C.-A., Anglés-Alcázar, D., et al. 2019, MNRAS,
   488, 1248
Hargis, J. R., Albers, S., Crnojević, D., et al. 2019, arXiv:1907.07185
Hasselquist, S., Carlin, J. L., Holtzman, J. A., et al. 2019, ApJ, 872, 58
Hinshaw, G., Larson, D., Komatsu, E., et al. 2013, ApJS, 208, 19
Homma, D., Chiba, M., Okamoto, S., et al. 2018, PASJ, 70, S18
Huang, S., Leauthaud, A., Murata, R., et al. 2018, PASJ, 70, S6
Hunter, J. D. 2007, CSE, 9, 90
Jacobs, B. A., Rizzi, L., Tully, R. B., et al. 2009, AJ, 138, 332
Jahn, E. D., Sales, L. V., Wetzel, A., et al. 2019, MNRAS, 489, 5348
Jang, I. S., & Lee, M. G. 2017, ApJ, 836, 74
Jerjen, H., Rekola, R., Takalo, L., Coleman, M., & Valtonen, M. 2001, A&A,
   380.90
Jethwa, P., Erkal, D., & Belokurov, V. 2016, MNRAS, 461, 2212
Jethwa, P., Erkal, D., & Belokurov, V. 2018, MNRAS, 473, 2060
Johnson, S. D., Chen, H.-W., Mulchaey, J. S., Schaye, J., & Straka, L. A. 2017,
    ApJL, 850, L10
Kalirai, J. S., Beaton, R. L., Geha, M. C., et al. 2010, ApJ, 711, 671
Kallivayalil, N., Sales, L. V., Zivick, P., et al. 2018, ApJ, 867, 19
Karachentsev, I., Kaisina, E., Kaisin, S., et al. 2011, MNRAS, 415, L31
Karachentsev, I., Makarov, D., & Kaisina, E. 2013, AJ, 145, 101
Karachentsev, I. D., & Kaisin, S. S. 2007, AJ, 133, 1883
Karachentsev, I. D., Karachentseva, V. E., & Huchtmeier, W. K. 2007, AstL,
Karachentsev, I. D., Sharina, M. E., Grebel, E. K., et al. 1999, A&A, 352, 399
Kawanomoto, S., Uraguchi, F., Komiyama, Y., et al. 2018, PASJ, 70, 66
Kereš, D., Katz, N., Weinberg, D. H., & Davé, R. 2005, MNRAS, 363, 2
Kim, D., & Jerjen, H. 2015, ApJL, 808, L39
Kim, S. Y., Peter, A. H. G., & Hargis, J. R. 2018, PhRvL, 121, 211302
Kirby, E. N., Cohen, J. G., Guhathakurta, P., et al. 2013, ApJ, 779, 102
Kirby, E. N., Lanfranchi, G. A., Simon, J. D., Cohen, J. G., & Guhathakurta, P.
   2011, ApJ, 727, 78
Komiyama, Y., Obuchi, Y., Nakaya, H., et al. 2018, PASJ, 70, S2
Laevens, B. P. M., Martin, N. F., Ibata, R. A., et al. 2015, ApJL, 802, L18
Leisman, L., Haynes, M. P., Janowiecki, S., et al. 2017, ApJ, 842, 133
Lelli, F., Verheijen, M., & Fraternali, F. 2014, MNRAS, 445, 1694
Lianou, S., Grebel, E. K., & Koch, A. 2010, A&A, 521, A43
Magnier, E. A., Schlafly, E., Finkbeiner, D., et al. 2013, ApJS, 205, 20
Martin, N. F., Ibata, R. A., Lewis, G. F., et al. 2016, ApJ, 833, 167
Martínez-Delgado, D., Romanowsky, A. J., Gabany, R. J., et al. 2012, ApJL,
  748, L24
Mayer, L., Mastropietro, C., Wadsley, J., Stadel, J., & Moore, B. 2006,
     INRAS, 369, 1021
McConnachie, A. W. 2012, AJ, 144, 4
McConnachie, A. W., Ibata, R., Martin, N., et al. 2018, ApJ, 868, 55
```

```
Merritt, A., van Dokkum, P., & Abraham, R. 2014, ApJL, 787, L37
Miyazaki, S., Komiyama, Y., Kawanomoto, S., et al. 2018, PASJ, 70, S1
Moster, B., Naab, T., & White, S. 2013, MNRAS, 428, 3121
Müller, O., Jerjen, H., & Binggeli, B. 2017, A&A, 597, A7
Nadler, E. O., Mao, Y.-Y., Green, G. M., & Wechsler, R. H. 2019, ApJ,
Nelson, D., Pillepich, A., Genel, S., et al. 2015, A&C, 13, 12
Nichols, M., & Bland-Hawthorn, J. 2011, ApJ, 732, 17
Oh, S.-H., de Blok, W. J. G., Walter, F., et al. 2008, AJ, 136, 2761
Papastergis, E., Cattaneo, A., Huang, S., Giovanelli, R., & Haynes, M. P. 2012,
Pardy, S. A., D'Onghia, E., Navarro, J., et al. 2019, arXiv:1904.01028
Pearson, S., Besla, G., Putman, M. E., et al. 2016, MNRAS, 459, 1827
Peñarrubia, J., Navarro, J., & McConnachie, A. 2008, ApJ, 673, 226
Price-Whelan, A. M. 2017, JOSS, 2, 388
Price-Whelan, A. M., Sipőcz, B. M., Günther, H. M., et al. 2018, AJ, 156, 123
Pucha, R., Carlin, J. L., Willman, B., et al. 2019, ApJ, 880, 104
Rich, R. M., Collins, M. L. M., Black, C. M., et al. 2012, Natur, 482, 192
Robitaille, T. P., Tollerud, E. J., Greenfield, P., et al. 2013, A&A, 558, A33
Rocha, M., Peter, A. H. G., & Bullock, J. 2012, MNRAS, 425, 231
Rodriguez-Gomez, V., Genel, S., Vogelsberger, M., et al. 2015, MNRAS,
Romanowsky, A., Martínez-Delgado, D., Martin, N., et al. 2016, MNRAS,
  457, L103
Ruiz-Lara, T., Beasley, M. A., Falcón-Barroso, J., et al. 2018, MNRAS,
  478, 2034
Sales, L. V., Navarro, J. F., Kallivayalil, N., & Frenk, C. S. 2017, MNRAS,
  465, 1879
Sales, L. V., Wang, W., White, S. D. M., et al. 2013, MNRAS, 428, 573
Sand, D., Crnojević, D., Strader, J., et al. 2014, ApJL, 793, L7
Sand, D. J., Spekkens, K., Crnojević, D., et al. 2015, ApJL, 812, L13
Schlafly, E. F., & Finkbeiner, D. P. 2011, ApJ, 737, 103
Schlafly, E. F., Finkbeiner, D. P., Jurić, M., et al. 2012, ApJ, 756, 158
Schlegel, D., Finkbeiner, D., & Davis, M. 1998, ApJ, 500, 525
Shipp, N., Drlica-Wagner, A., Balbinot, E., et al. 2018, ApJ, 862, 114
Simon, J. D. 2019, ARA&A, 57, 375
Slater, C. T., & Bell, E. F. 2014, ApJ, 792, 141
Smercina, A., Bell, E. F., Price, P. A., et al. 2018, ApJ, 863, 152
Spekkens, K., Urbancic, N., Mason, B., Willman, B., & Aguirre, J. 2014,
   ApJL, 795, L5
Stierwalt, S., Besla, G., Patton, D., et al. 2015, ApJ, 805, 2
Taylor, M. 2005, in ASP Conf. Ser. 347, Astronomical Data Analysis Software
  and Systems XIV, ed. P. Shopbell, M. Britton, & R. Ebert (San Francisco,
  CA: ASP), 29
Toloba, E., Sand, D. J., Spekkens, K., et al. 2016, ApJL, 816, L5
Tonry, J. L., Stubbs, C. W., Lykke, K. R., et al. 2012, ApJ, 750, 99
Torrealba, G., Belokurov, V., Koposov, S. E., et al. 2018, MNRAS, 475, 5085
Torrealba, G., Koposov, S. E., Belokurov, V., et al. 2016, MNRAS, 463, 712
Tully, R. B., Courtois, H. M., & Sorce, J. G. 2016, AJ, 152, 50
van der Walt, S., Colbert, S. C., & Varoquaux, G. 2011, CSE, 13, 22
Vogelsberger, M., Genel, S., Sijacki, D., et al. 2013, MNRAS, 436, 3031
Vogelsberger, M., Genel, S., Springel, V., et al. 2014a, MNRAS, 444, 1518
Vogelsberger, M., Genel, S., Springel, V., et al. 2014b, Natur, 509, 177
Wang, M. Y., de Boer, T., Pieres, A., et al. 2019, ApJ, 881, 118
Weisz, D. R., Dalcanton, J. J., Williams, B. F., et al. 2011, ApJ, 739, 5
Wetzel, A. R., Hopkins, P. F., Kim, J.-H., et al. 2016, ApJL, 827, L23
Wetzel, A. R., Tollerud, E. J., & Weisz, D. R. 2015, ApJL, 808, L27
Williams, B. F., Dalcanton, J. J., Stilp, A., et al. 2013, ApJ, 765, 120
Willman, B., Dalcanton, J., Martínez-Delgado, D., et al. 2005, ApJL, 626, L85
Woo, J., Courteau, S., & Dekel, A. 2008, MNRAS, 390, 1453
York, D. G., Adelman, J., Anderson, J. E., et al. 2000, AJ, 120, 1579
Zolotov, A., Brooks, A. M., Willman, B., et al. 2012, ApJ, 761, 71
```